Spatial gradient of total electron content (TEC) between two nearby stations as indicator of occurrence of ionospheric irregularity

Teshome Dugassa[1, 2], John Bosco Habarulema[3, 4], and Melessew Nigussie[5]

[1]Ethiopian Space Science and Technology Institute (ESSTI), Addis Ababa, Ethiopia
[2]Bule Hora University, College of Natural and Computational Science, Department of Physics, Bule Hora, Ethiopia
[3]South African National Space Agency (SANSA), Space Science, 7200, Hermanus, South Africa.
[4]Department of Physics and Electronics, Rhodes University, 6140, Grahamstown, South Africa.
[5]Washera Geospace and Radar Science Laboratory, Physics Department, Bahir Dar University, Bahir Dar, Ethiopia

Correspondence: Teshome Dugassa (tdugassa2016@gmail.com), John Bosco Habarulema (jhabarulema@sansa.org.za), Melessew Nigussie (melessewnigussie@yahoo.com)

1 **Abstract.** The relation between the occurrence of ionospheric irregularity and spatial gradient of total electron content
2 (TEC) during the post-sunset hours over the equatorial region is studied. The ionospheric irregularities could pose se-
3 rious challenges to satellite-based navigation and positioning applications when trans-ionospheric signals pass through
4 them. Different instruments and techniques have been applied to study the behavior of these ionospheric irregularities.
5 In this study, the Global positioning system (GPS) based derived total electron content (TEC) was used to investigate
6 the spatial gradient of TEC between two nearby stations as indicator of occurrence of ionospheric irregularity over the
7 East African sector. The gradient of TEC between the two stations (ASAB: $4.34°$ N, $114.39°$ E and DEBK: $3.71°$ N,
8 $109.34°$ E, geomagnetic) located within the equatorial region of Africa were considered in this study during the year
9 2014. The rate of change of TEC based derived index ($ROTI_{ave}$) is also used to observe the correlation between the
10 spatial gradient of TEC and the occurrence of ionospheric irregularities. The result obtained shows that most of the
11 maximum positive/depletions in the spatial gradient of TEC observed in March and September equinoxes are more pro-
12 nounced between 19:00 LT - 24:00 LT as the large-scale ionospheric irregularities do. Moreover, the observed spatial
13 gradient of TEC shows two peaks (in March and September) and they exhibit equinoctial asymmetry where the March
14 equinox is greater than September equinox. The enhancement in the spatial gradient of TEC and $ROTI_{ave}$ during the
15 evening time period also show similar trends but lag 1-2 hrs from the equatorial electric field (EEF). The spatial gra-
16 dient of TEC between the two nearby stations could be used as an indicator of the occurrence of ionospheric irregularities.

18 **Key words**: Spatial gradient of TEC, $ROTI_{ave}$, ionospheric irregularities

1 Introduction

The ionosphere is a dispersive medium in which radio signals are refracted depending upon signal frequency and ionospheric density. After sunset, the ionospheric plasma interchange instabilities present in the equatorial/low-latitude ionosphere generate large-scale depletions in the ambient electron density which leads to the formation of plasma density irregularities that affect radio communication and navigation system (Basu and Basu, 1981). The generation of the plasma irregularities can be related to the lack of plasma production immediately after sunset and the fast recombination rate in the E-region ionosphere, which results in a steep gradient in electron density. In the evening hours, the large enhancement of F region vertical plasma drift attest to the presence of enhanced eastward electric field is also another parameter which controls the generation of plasma density irregularities (Fejer, 1991; Fejer et al., 2008). This prereversal enhancement in the vertical plasma drift moves the F region to higher altitudes (Abdu et al., 2009). When the altitude of F-region is high enough to overcome recombination effects, the Rayleigh-Taylor instability mechanisms initiates a growth in plasma fluctuations. Kelley (2009) reported that the existence of equatorial plasma bubbles (EPB) is attributed to the instability of the Rayleigh-Taylor (R-T) plasma which is triggered by the intensification of the eastward equatorial electric field just before its reversal. The R-T instability mechanism is considered the primary mechanism responsible for the generation of ionospheric plasma density irregularities or plasma bubbles in equatorial and low-latitude region (Rao et al., 2006; Fejer et al., 1999). A perturbation at the base of the F-region, such as that caused by a gravity wave, can also lead to the growth of the instability, resulting in the formation of plasma bubbles, that is, structures with depleted plasma density that produce ESF (Abdu, 2001; Abdu et al., 2009; Kelley, 1989).

Several studies have indicated that ionospheric irregularities show strong diurnal, seasonal, geographic and solar cycle variations (Chu et al., 2005; Kintner et al., 2007). Longitudinal and geomagnetic activity dependency of ionospheric irregularities over the different equatorial region has also been reported (Burke et al., 2004; Susnik and Forte, 2011; Paznukhov et al., 2012; Oladipo and Schuler, 2013a; Seba and Tsegaye, 2015). Oladipo and Schuler (2013a) studied large-scale ionospheric irregularities at Franceville, Gabon, an equatorial station in the African sector for a year (2001/2002) during the last high-solar activity. Their results showed the seasonal dependency of the occurrence of ionospheric irregularities. Furthermore, the study of Seba and Tsegaye (2015) showed seasonal and annual scintillation characteristics over Bahir Dar, Ethiopia. Also, they indicate that the high-level intensity of scintillation occurred in March and April, and was low on Solstice days. Tsunoda (1985) proposed that the seasonal and longitudinal occurrences of the plasma bubble are most frequent when the solar terminator is most closely aligned with the geomagnetic meridian.

In the past years, several techniques both from the ground and space-based instruments have been used to study the occurrence of ionospheric irregularities. The widely used instrument was the GPS scintillation index, S4. In the recent years, GNSS (Global Navigation Satellite System) based technique has become an important tool for the study the behavior of ionospheric irregularities (Pi et al., 1997; Nishioka et al., 2008) because of its growing application in civilian and military applications. Using ground-based GPS measurements over African equatorial and low-latitude regions, the

1 seasonal occurrence of the ionospheric irregularities has been studied by the several workers (Olwendo et al., 2013, 2016;

2 Ngwira et al., 2013; Seba and Tsegaye, 2015; Oladipo and Schuler, 2013b; Oladipo et al., 2014; Mungufeni et al., 2016).

3 The ionospheric irregularities have adverse effects on trans-ionospheric signals. Therefore, forecasting the probability of

4 occurrence of ionospheric irregularities has become the topic of major research and has drawn the attention of the scientific

5 community. Due to these effects, modeling ionospheric irregularities has been carried out by several researchers (Aarons,

6 1985; Scherliess and Fejer, 1999; Abdu et al., 2003; Iyer et al., 2006; Mungufeni et al., 2015; Taabu et al., 2016). Aarons

7 (1985) developed an analytical equation to yield scintillation excursions based on a series of observations at 254 MHz

8 taken at Huancayo, Peru, as a function of different parameters. Abdu et al. (2003) developed a regional model for the quiet

9 time spread-F distribution in the Brazilian longitude sector. Iyer et al. (2006) developed an empirical model of magnetic

10 quiet time scintillation occurrence at Indian equatorial and low-latitudes. Mungufeni et al. (2015) developed an empirical

11 model for the probability of occurrence of ionospheric irregularities during geomagnetic quiet conditions over the African

12 equatorial region. Moreover, Taabu et al. (2016) predicts ionospheric scintillation over East African region using neural

13 network during the ascending phase of sunspot cycle 24.

14 The evening prereversal enhancement (PRE) of the vertical plasma drift has important consequences for the Appleton

15 density anomaly and the stability of the nighttime ionosphere. Studies show that the occurrence of ESF is dependent on

16 an increase with maximum $E \times B$ drift velocity (Whalen, 2001). Using multi-instrument observation, Dabas et al. (2003)

17 suggested that the equatorial electrojet (EEJ) is a useful parameter for predicting the EPBs development. The PRE in the

18 eastward electric field component near sunset in the equatorial ionosphere is a phenomenon that has been well reported

19 and studied (see., Kelley, 2009). Several theories have been proposed to explain the PRE (Rishbeth, 1971; Farley et al.,

20 2008; Haerendel and Eccles, 1992). Low-latitude/equatorial F-region vertical plasma drifts have been measured extensively

21 using coherent and incoherent scatter radar measurements at the Jicamarca Radio Observatory and they have also been

22 inferred from daytime magnetometer (e.g., Anderson et al., 2004) and nighttime ionosonde observations (e.g., Abdu et al.,

23 1981). It has been suggested that the longitudinal gradient of integrated Pederson conductivity in the E-region at sunset

24 time can play a positive role in strengthening the evening pre-reversal enhancement magnitudes (Tsunoda, 1985; Batista

25 et al., 1986). However, over African longitude sector, it may not be easy to have the longitudinal gradient of electron

26 density as ionosondes are not available in nearby locations and see the correlation between electron density gradient and

27 occurrence of irregularities. A closely found GPS receivers may be a good option to investigate the relation between

28 longitudinal gradient of total electron content derived from GPS receivers and occurrence of ionospheric irregularities.

29 In the present study, we investigate the longitudinal gradient of total electron content derived from two close by GPS

30 stations over Ethiopia (Debark) and Eritrea (Asab) as indicator of occurrence of ionospheric irregularities, and discuss the

31 probability of occurrence of ionospheric irregularities. The relation between the daytime eastward equatorial electric field

32 derived from the equatorial electric field (EEF) model and the daytime equatorial electrojet derived from magnetometer

33 measurements will be discussed.

1 ## 2 Data and analysis method

2 The present study has been carried out using receiver-independent exchange (RINEX) data from dual frequency GPS

3 receivers located at Debark, Ethiopia and Asab, Eritrea obtained from (http://www.unavco.org/data/gps-gnss/data).

4 The GPS-TEC program developed at Boston College (Seemala and Valladares, 2011) was applied to derive TEC values

5 from each dual frequency GPS receiver. The study focuses on the year 2014. In order to avoid the multipath effects,

6 different authors have used observation data of above certain cutoff mask ranging from $15°$ to $35°$ (Chu et al., 2005;

7 Mushini and Pokhotelov, 2011). In the current study, we used an elevation cutoff mask of $30°$. Average VTEC values

8 are obtained by averaging VTEC over 30 min interval for all satellites in view with elevation angle above $30°$. Using the

9 GPS-TEC data collected from these two receiver stations, the spatial gradient of TEC (the difference of TEC between

10 the two receivers) were computed for every time and then analyzed to show the possible indicator of F-region ionospheric

11 irregularity occurrence. The spatial gradient of TEC between the two nearby stations are located nearly along the same

12 geographic latitude with longitudinal separation of about $\sim 5°$ or corresponding spatial separation of 535.7 km were

13 computed using Eq. (1).

14 $$Spatial\ gradient\ of\ TEC(t) = \frac{VTEC_{asab}(t) - VTEC_{debk}(t)}{d} \tag{1}$$

15 where d represents the separation distance between the two stations.

16 ΔH values (ΔH refers to the deviation of the horizontal component of the earth's magnetic field H from its mean night

17 time level) at Addis Ababa and Adigrat have also been used for this study in computing the equatorial electrojet (EEJ).

18 Table 1 gives the list of all the stations for which data has been used in this study.

Table 1. Location information and the type of data used in this study.

Name of stations	Code	Geo. lon	Geo. lat	Geom. lon	Geom. lat	Data
Asab, Eritrea	ASAB	$42.65°$ E	$13°$ N	$114.34°$ E	$4.85°$ N	GPS-TEC
Debark, Ethiopia	DEBK	$37.65°$ E	$13°$ N	$109.24°$ E	$4.13°$ N	GPS-TEC
Addis Ababa, Ethiopia	AAE	$38.77°$ E	$9.04°$ N	$110.47°$ E	$0.18°$ N	Magnetometer
Adigrat, Ethiopia	ETHI	$39.46°$ E	$14.28°$ N	$111.06°$ E	$5.80°$ N	Magnetometer

19 The other data source used in this study was the Real-time model of the Ionospheric Electric Fields (http://geomag.org/

20 models/PPEFM/RealtimeEF.html). We have used this model to observe the relation between the equatorial electric field

21 (EEF) and the spatial gradient of TEC between the two receivers. The Prompt Penetration Electric Field Model (PPEFM)

22 (Manoj and Maus, 2012) is a transfer function model which to models the daily variations coming from the solar wind,

which are mapped from interplanetary electric field (IEF) data. Eight (8) years IEF data from the ACE satellite, radar data from JULIA, and magnetometer data from the CHAMP satellite was used to derive the transfer function. Using the real-time data from ACE satellite, the transfer function models the current variations in the equatorial ionospheric electric fields. The model takes time and location as input parameters and calculates the best estimates of the equatorial electric field. In the present study, we have used only the background quiet-time electric field.

Recently, Nayak et al. (2017) used the real-time model of electric field to observe the influence of prompt penetration electric field (PPEF) on the occurrence of ionospheric irregularities during 17 March 2015 geomagnetic storm over Indian and Taiwan longitudes. This model has not been applied yet to explain the electrodynamic phenomena over African low-latitude region. To use this model in this region, we first observed the relation between the daytime of quiet time equatorial electric field (EEF) and equatorial electrojet (EEJ), which has a direct relation with $E \times B$ vertical drift. To do this, ground based magnetometer stations one located at magnetic equator and another one at $(6° - 9°)$ off-equator (Rastogi and Klobuchar, 1990; Anderson et al., 2002; Yizengaw et al., 2014) have been used. Over East Africa there were two magnetometer stations, one at Adigrat, (ETHI, $14.3°$ N, $39.5°$ E, $6.0°$ N geomagnetic) and the other at Addis Ababa, (AAE, $9.0°$ N, $38.8°$ E, $0.2°$ N geomagnetic). ETHI and AAE stations belong to African Median and B-Filed Education research, (AMBER) network (Yizengaw and Moldwin, 2009) and International Magnetic Network (INTERMAGNET), respectively. The difference of the horizontal component (H) of geomagnetic field of these station, ΔH gives the equatorial electrojet contribution which is a proxy to daytime electric field. The connection between the occurrence of ESF during evening sector preceded by the rapid rise in F-layer and the strength of EEJ before sunset has been presented (Kelley, 2009; Burke et al., 2004). Sreeja et al. (2009) reported observational evidence for the plausible linkage between the EEJ electric field variations with the postsunset F-region electrodynamics. Furthermore, Hajra et al. (2012) indicate that the afternoon/evening time variation of eastward electric field as revealed through EEJ seems to play dominant role in dictating postsunset resurgence of EIA and consequent generation of spread-F irregularities. Once the relation between equatorial electric field model and is ΔH determined, and the model is found to be reliable the equatorial electric field derived from the model will be used in this study to explain the gradient of TEC and occurrence of irregularities.

We also used rate of change of TEC derived index ($ROTI_{ave}$) to observe the presence of ionospheric irregularities. The time variation of TEC also known as rate of change of TEC (ROT) and its derived indices are a good proxy for the phase fluctuation, which is a measure of large-scale ionospheric irregularities (Aarons et al., 1997). These kinds of indices can be used to characterize all the known features of equatorial spread F (ESF) (Mendillo et al., 2000). The rate of change of TEC (ROT) is given by

$$ROT = \frac{TEC_k^i - TEC_{k-1}^i}{t_k^i - t_{k-1}^i} \qquad (2)$$

where i is the visible satellite and k is the time of epoch and ROT is in units of TECU/min. The ROTI was introduced by Pi et al. (1997) to statistically quantify the ROT measurements. The ROTI is defined as the standard deviation of ROT

1 over a 5-min period. Usually, ROTI > 0.5 TECU/min indicates the presence of ionospheric irregularities at scale lengths

2 of a few kilometers Ma and Maruyama (2006).

3 $$ROTI = \sqrt{\langle ROT^2 \rangle - \langle ROT \rangle^2}$$ (3)

4 where ROT can be obtained from Eq. (2). Oladipo and Schuler (2013b) employed the idea of Mendillo et al. (2000) to

5 obtain a new index called $ROTI_{ave}$ index given in Eq. (4). $ROTI_{ave}$ index is the average of ROTI over 30 min interval

6 for a satellite and then average over all satellites in view. The index gives average level of irregularities over half an

7 hour. Recently, Oladipo et al. (2014) used $ROTI_{ave}$ to demonstrate and capture the level of ionospheric irregularity over

8 Nigeria. In this study, the rate TEC fluctuation index (ROTI) (Pi et al., 1997; Oladipo and Schuler, 2013b; Oladipo et al.,

9 2014) were used to observe the occurrence of irregularities the stations.

10 $$ROTI_{ave}(0.5hr) = \frac{1}{N}\sum_{n=1}^{N}\sum_{i=1}^{k}\frac{ROTI(n,0.5hr,i)}{k}$$ (4)

11 where n is the satellite number, $0.5hr$ is half an hour (0, 0.5, 1,... 23.5, 24 UT), i is the 5 min section within half an

12 hour (i = 1, 2, 3, 4, 5, 6), N is the number of satellites observed within half an hour and k is the number of $ROTI$

13 values available within half an hour for a particular satellite. According to Oladipo and Schuler (2013b), the value of

14 $ROTI_{ave} < 0.4$, $0.4 < ROTI_{ave} < 0.8$ and $ROTI_{ave} > 0.8$, respectively represents the background fluctuation, existence

15 of phase fluctuation, and severe phase fluctuation activities. In the present study, these threshold values of $ROTI_{ave}$

16 index were used to statistically observe the occurrence of ionospheric irregularities and compare with the spatial gradient

17 of TEC between the two nearby stations.

18 **3 Results and Discussions**

19 **3.1 Relation between the day-time Equatorial Electrojet (EEJ) and Equatorial Electric Field Model (EEFM)**

20 Figure 1a presents typical example of the diurnal variation of equatorial electric field and equatorial electrojet on 26 March

21 2012 while Fig. 1b shows the correlation between the equatorial electrojet derived from (ΔH) and equatorial electric field

22 (EEF) derived from equatorial electric field model in the daytime period (07:00 to 17:00 LT) for some of selected quiet days

23 of month of the year 2012. The equatorial electric field is a key factor in determining the dynamics and structure of the

24 low latitude ionosphere (Fejer, 2011). For the first time it was detected by the Jicamarca (11.95° S, 76.87° W) incoherent

25 scatter radar (ISR) and the Jicamarca Unattended Long-Term studies of the Ionosphere and Atmosphere (JULIA) system

26 during the period from 1998 to 2008. However, there were no direct continuous electric field observations from ground

27 based and when available, mostly limited to the daytime. Over African region there is no ground based measurements

28 of the zonal electric fields. Anderson et al. (2002) used the ΔH deduced from magnetometers and vertical plasma drifts

1 observed by Jicamarca ISR to identify a positive and linear relationship between the equatorial EEJ and EEF. Since then,

2 the ΔH is widely known as a substitution for the EEF. To use the ΔH derived from the horizontal (H) component of

3 geomagnetic field over East African sector, AMBER magnetometer data over Adegrat, Ethiopia (ETHI) station during the

4 year 2014 were not available. To solve this data gap we used the daytime information of equatorial electric field derived

5 from the real-time prompt penetration electric field model as an option. The relation between the daytime (07:00 - 17:00

6 LT) value of ΔH deduced from magnetometers and the equatorial electric field obtained from EEFM during the year 2012

7 were presented in Fig. 1b. As shown in the figure, the daytime equatorial electrojet (ΔH) correlate linearly with quiet-time

8 equatorial electric field model with correlation coefficient of (R = 0.70). Studies showed that the daytime electrodynamics

9 play a decisive role in the initiation of post-sunset ESF (e.g., Mendillo et al., 2001; Valladares et al., 2001, 2004). Hence,

10 in this study we have used the equatorial electric field derived from EEFM model to show its effect on the post-sunset

11 enhancement of the spatial gradient of TEC and explain the possibility that it could be used as indicator of occurrence of

12 ionospheric irregularities.
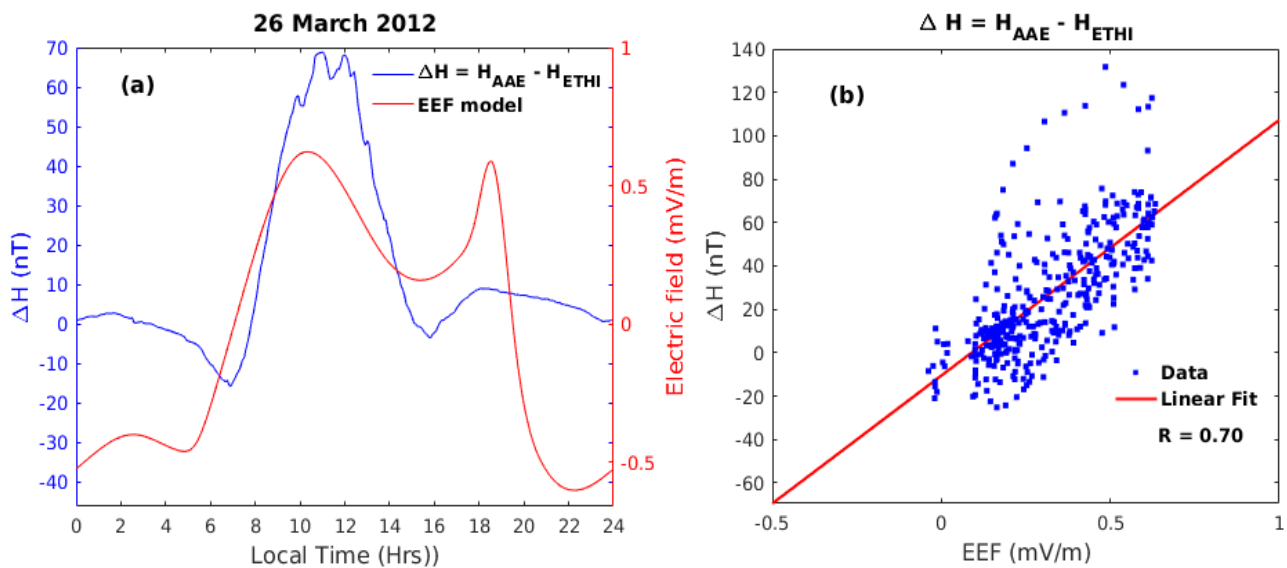
Figure 1. (a) Diurnal variation of Equatorial Electric field Model (EEF) and ΔH and (b) Day-time correlation between the equatorial electrojet (EEJ) and quiet-time equatorial electric field model (EEF) for quiet days of month of year 2012.

3.2 Relation between the equatorial electric field (EEF), the spatial gradient of TEC and occurrence of ionospheric irregularities

Figure 2a and d present examples showing the relation between an enhancement in the spatial gradient of TEC and the equatorial electric field during the pre-midnight period. The red and blue curve indicates the equatorial electric field and the spatial gradient of TEC, respectively. From Fig. 2, it can be observed that the equatorial electric field start rising nearly after 16:00 LT and enhanced in the evening local time at about 18:00 LT. Most of the enhancement of the spatial gradient of TEC was also observed in the evening local time (18:00 - 24:00) but lags 1-2 hours from the post-sunset enhancement of the equatorial electric field. The depletions in the gradient of TEC (not shown here) also shows a similar trend with the equatorial electric field as the maximum positive of the spatial gradient of TEC does. The spatial gradient of TEC observed during the daytime was relatively small compared to the evening time value for most of the days. The maximum enhancement/depletion in the gradient of TEC observed in the evening period could be related to the pre-reversal enhancement in zonal electric field. Mendillo et al. (2001) have pointed out that the best available precursor for pre-midnight ESF is the EIA strength at sunset. Using differential TEC profiles, TEC (at 1800 h) - TEC (at 2000 h), Valladares et al. (2004) explained that the pre-reversal enhancement (PRE) of the vertical drift would reenergize the fountain effect.

Typical examples showing the relation between the spatial gradient of TEC and the phase fluctuation index indicated by $ROTI_{ave}$ showing the occurrence of ionospheric irregularities is depicted in Fig. 3a - d. The blue and the red curves, respectively, indicate the spatial gradient of TEC between the two GPS stations and the phase fluctuation index ($ROTI_{ave}$) over Asab. In the post-sunset hours, after 18:00 LT, the pattern of the two parameters shows a similar trend. The enhancement in the gradient of TEC and occurrence of irregularities in the post-sunset period could be explained by the presence of ionospheric electrodynamics. The post-sunset period electrodynamics is influenced by F-region dynamo which is governed by a longitudinal gradient of the electrical conductivity and thermospheric zonal wind (Crain et al., 1993). Anderson et al. (2004) showed that the scintillation activity is related to the maximum $E \times B$ drift velocity between 1830 and 1900 LT.

It has been reported that the eastward component of electric field manifested by the vertical plasma drifts over equator and intensified around/shortly after sunset before reversing to westward is one of the most important parameters responsible for driving many interesting ionospheric phenomena, like the Appleton density anomaly and the stability of the nighttime ionosphere (e.g., Horvath and Essex, 2003; Abadi et al., 2015). In the evening sectors, the vertical drift enhancement is of particular significance as it is the major drivers for the generation of ESF (Farley et al., 1970; Woodman, 1970; Basu et al., 1996; Fejer et al., 1999; Martinis et al., 2005). Tulasi Ram et al. (2006) reported that the rapid enhancement of post-sunset of the zonal electric field leads to a large vertical plasma drift ($E \times B$), thereby lifting the F-layer to higher altitudes resulting in a condition conducive for the generation of ESF. Vertical drifts are taken as the key parameters determining the dynamics of ionospheric F-region, and the occurrence of ESF. Ionospheric irregularities are mostly observed over
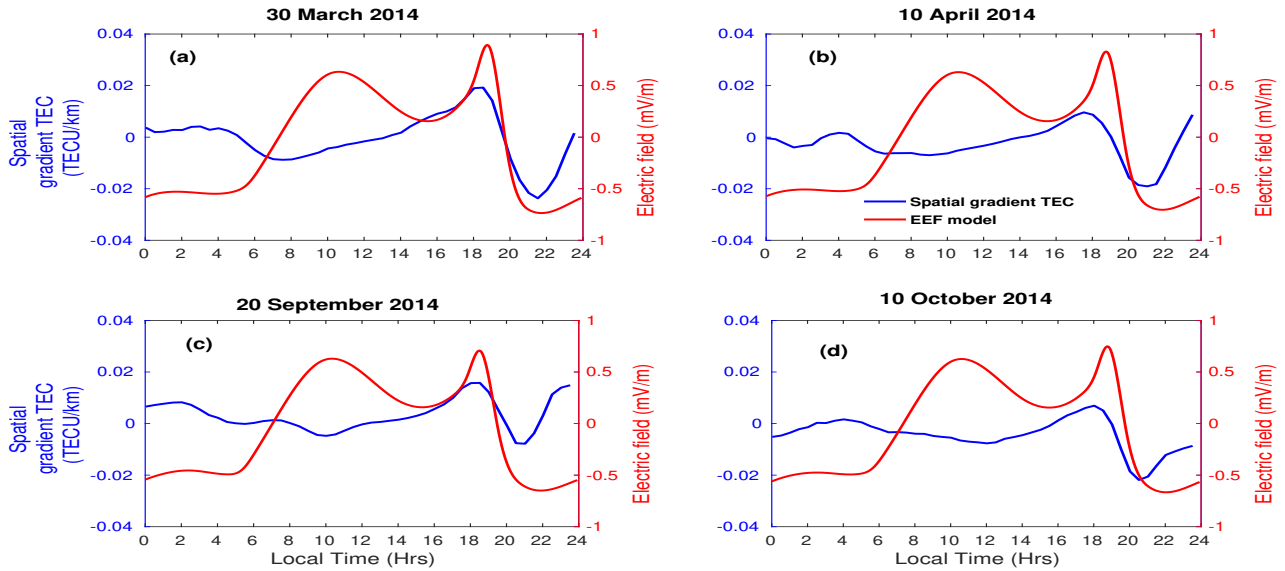
Figure 2. An example of comparison of equatorial electric field model (EEFM) and the spatial gradient of TEC on a) 30 March 2014, b) 10 April 2014, c) 20 September 2014 and b) 10 October 2014.
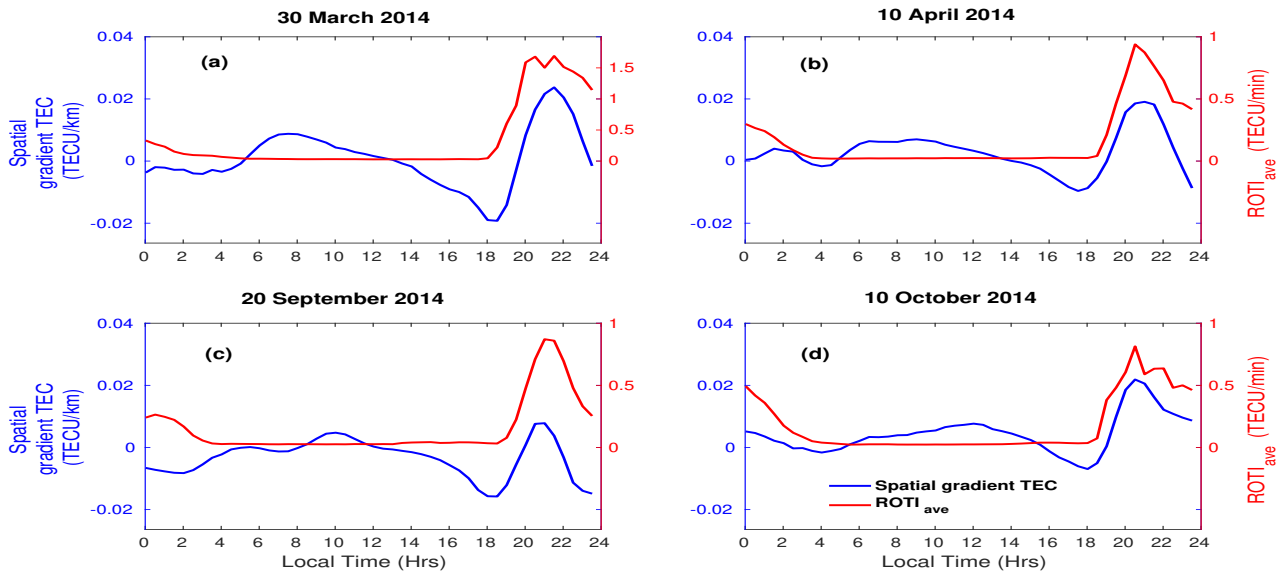
Figure 3. An example showing relation between the patterns of the spatial gradient of TEC and the $ROTI_{ave}$ on a) 30 March 2014, b) 10 April 2014, c) 20 September 2014 and b) 10 October 2014.

1 equatorial/low-latitude region an hour or two hours after the pre-reversal enhancement (PRE). From the figure, the post-
2 sunset enhancement in zonal electric field as shown in the equatorial electric field model has a profound effect on the
3 enhancement of the spatial gradient of TEC during the post-sunset period. This might indicate that the spatial gradient
4 of TEC as indicator of occurrence of ionospheric irregularities. Different researchers used the concept of ionosphere spatial
5 gradient based on multi-GNSS observations within a small scale region to provide corrections and integrity information
6 to the Ground-Based Augmentation System (GBAS) and they attribute the large ionosphere spatial gradient to the TEC
7 enhancements and the ionosphere irregularities (Rungraengwajiake et al., 2015; Saito and Yoshihara, 2017). An ionosphere
8 gradient of 518 mm/km was discovered, generated by a plasma bubble (Saito and Yoshihara, 2017).

9 Figure 4a and b, respectively, show the annual plots of phase fluctuation at Asab and Debark indicated by $ROTI_{ave}$ index
10 during the year 2014. The $ROTI_{ave}$ values are indicated in color scale. The occurrence of ionospheric irregularities at the
11 two stations, as indicated by $ROTI_{ave}$ value, is a post-sunset phenomenon. The implication of this is that the large-scale
12 ionospheric irregularities, which are responsible for the scintillation of transionospheric signals at GNSS frequencies, are
13 more pronounced during post-sunset hours. The observed phase fluctuation shows monthly variations and there is also a
14 seasonal trend in the occurrence of ionospheric irregularity (see., Fig. 5). Maximum irregularities were observed in March
15 equinox months and minimum in June/July. During this period, the occurrence of phase fluctuation showing irregularities is
16 observed mainly between 19:00 LT and 24:00 LT. As stated by Oladipo and Schuler (2013b), the value of $ROTI_{ave} > 0.4$
17 shows a presence of ionospheric irregularity.

18 Figure 4c indicates the annual plots of the spatial gradient of TEC between the two nearby GPS stations, Debark (DEBK)
19 and Asab (ASAB) during the year 2014. As already stated in section (2), the two stations are located nearly on the
20 same geographic and geomagnetic latitudes with a longitudinal separation of about $5°$ or corresponding spatial separation
21 of about 535.7 km. In the computation of the spatial gradient of TEC (Using Eq. 1), negative and positive values of
22 the gradient of TEC were observed. From the figure, the maximum positive/negative value of the gradient of TEC was
23 observed mostly during the post-sunset (18:00 - 24:00 LT) and postmidnight (24:00 - 06:00 LT) period. Equation (1) was
24 applied to all days of the year 2014 in computing the spatial gradient of TEC. Out of total of observed daily maximum
25 value of gradient of TEC, about 194 days (in percent about 53 %) of them fall in this time period intervals. There was
26 also a case where the maximum positive and depletions in the value of gradient of TEC were observed in the early morning
27 period.

28 The positive enhancement in the gradient of TEC observed during post-sunset and postmidnight showing monthly and
29 seasonal variations are the other features noticed from Fig. 4c. The values of the spatial gradient of TEC observed on
30 equinoctial months was greater than Solstice months. Equinoctial asymmetry in the occurrence of TEC gradient was also
31 observed, where March equinox is greater than September equinox. Similarly, the depletions of the spatial gradient of TEC
32 are mostly observed during post-sunset and post-midnight periods as the maximum positive TEC gradient. The depletions
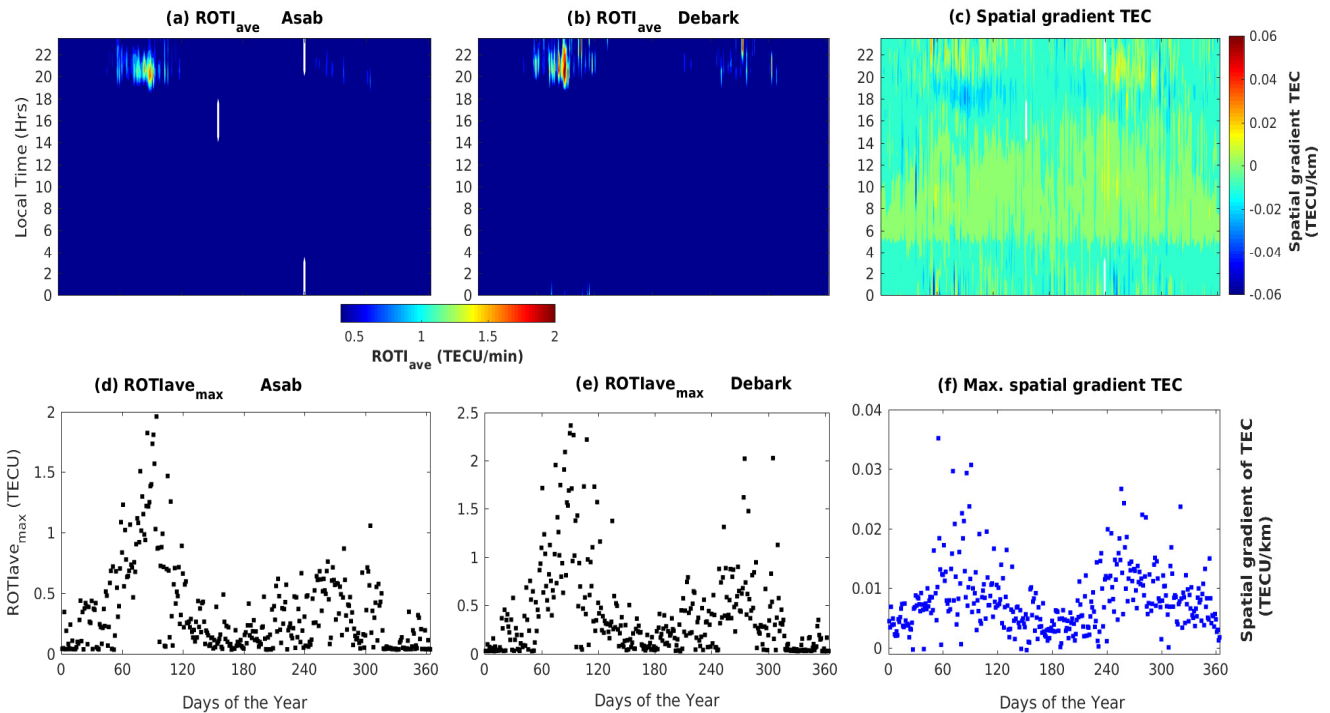
Figure 4. a) Diurnal variation of the spatial gradient of TEC over ASAB and DEBK , b) Daily maximum value of the spatial gradient of TEC variation, c) Diurnal variation of $ROTI_{ave}$ over ASAB station and d) Daily maximum value variation of $ROTI_{aave}$ over ASAB station in the year 2014

1 of the gradient of TEC observed during the year 2014 also shows equinoctial asymmetry where the March equinoxes were

2 greater than September equinoxes (not shown).

3 Figure 4d and e present the daily maximum phase fluctuation index, $ROTI_{ave}$, over Asab and Debark stations, respectively

4 and Fig. 4f shows the daily maximum of the gradient of TEC during the year 2014. It is clearly observed from the figures

5 that the enhancement in $ROTI_{ave}$ and gradient of TEC shows monthly and seasonal variations, and the equinoctial

6 asymmetry was also observed. To identify whether the spatial gradient of the total electron content (TEC) between the

7 two nearby stations indicate the occurrence probability of ionospheric irregularity, the rate of change of TEC derived

8 index ($ROTI_{ave}$) described in section (2) expressed by Equation (4) and the spatial gradient of TEC between the two

9 receivers were compared. The daily maximum value of the spatial gradient of TEC between the two stations shows similar

10 trends with the daily maximum value of $ROTI_{ave}$ observed over ASAB and DEBK stations. The trend they show has

11 similarity with the time of occurrence of maximum enhancement, monthly and seasonal variations. Moreover, the seasonal

12 variation observed in both variables exhibits equinoctial asymmetry, where the March equinox was greater than September

13 equinoxes. The mechanism of generation of the enhancement in vertical drift just after sunset was detailed by Farley et al.

1   (2008). The magnitude of peak vertical drift is known to control the seasonal and day-to-day variations in the occurrence

2   of equatorial spread F (Manju et al., 2009; Tulasi Ram et al., 2006).

3   Figure 5 presents the percentage occurrence of ionospheric irregularities over ASAB in the year 2014. The percentage

4   occurrence of irregularities was calculated by counting the number of days in a month with $ROTI_{ave} \geq 0.4$ TECU/min

5   and dividing by the number of days in a month for which data are available, and multiplied by 100 %. The two peaks

6   of irregularity seasons occur around the middle of the equinoxes (i.e., in March and September) were observed at this

7   station. Previous studies indicated that the seasonal and day-to-day variations in the occurrences of EPB depend on the

8   geographical longitude and latitude. The maximum occurrence of EPB was observed during the equinoxes at longitudes

9   where the magnetic field lines aligned with a geographic meridian (Burke et al., 2004; Tsunoda, 2005, 2010). The

10   seasonal variation of ionospheric irregularities exhibit an equinoctial asymmetry in its occurrence especially at the two

11   peaks (i.e., in March and September), where March equinox is greater than that of September equinox. Based on a

12   few station observations, earlier studies indicated that equinoctial asymmetry in the occurrence of L-band scintillations

13   may be attributed to differences in the meridional winds during two equinoxes (e.g., Nishioka et al., 2008; Maruyama

14   et al., 2006; Otsuka et al., 2006). Nishioka et al. (2008) have shown the occurrence characteristics of plasma bubbles

15   using GPS TEC obtained all over the globe and found equinoctial asymmetry in the occurrence of plasma bubbles in

16   the Asian region. They have suggested that equinoctial asymmetry could be due to asymmetric distribution of integrated

17   conductivities during these equinoctial periods. Using three ionosondes observations Maruyama et al. (2006) reported

18   that meridional wind is the key factor for the equinoctial asymmetry. Using multi-instrument observations, Sripathi et al.

19   (2011) examined the equinoctial asymmetry in scintillation occurrence in the Indian sector and proposed the asymmetry

20   in the electron density distribution and meridional winds as possible causative mechanism. Manju (2013) also reported

21   equinoctial asymmetry in ESF occurrence and discussed the possible role of asymmetric meridional winds. Dasgupta et al.

22   (1983) studied the equinoctial asymmetry in equatorial and low latitude F region ionization distribution and attributed

23   it to neutral composition changes. Manju and Haridas (2015) observed significant asymmetry in the threshold height

24   between the vernal equinox and autumn equinox and underlines the distinct differences in the role of neutral dynamics

25   in ESF triggering during the two equinoxes. The local time and seasonal trends of occurrence of ionospheric irregularities

26   observed in this study are similar to those reported in the previous studies (Aarons, 1993; Basu et al.; Olwendo et al., 2013;

27   Amabayo et al., 2014; Seba and Tsegaye, 2015). The occurrence of equatorial F-region irregularity has been studied, and

28   the frequency of occurrence of equatorial spread F has been found to be higher during solar maximum (Abdu et al., 1998;

29   Mendillo et al., 2000). Similarly, Susnik and Forte (2011); Paznukhov et al. (2012); Oladipo and Schuler (2013b); Oladipo

30   et al. (2014); Mungufeni et al. (2016) reported the seasonal and equinoctial asymmetry in the occurrence of ionospheric

31   irregularities over African low-latitude sector based on scintillation index (S_4) and GPS-TEC derived index. The maximum

32   $ROTI_{ave}$ observed over this station in the year 2014 was about 1.8 TECU/min in March 2014. It is evident from Fig. 5

33   that the minimum level of $ROTI_{ave}$ was observed on December Solstice.
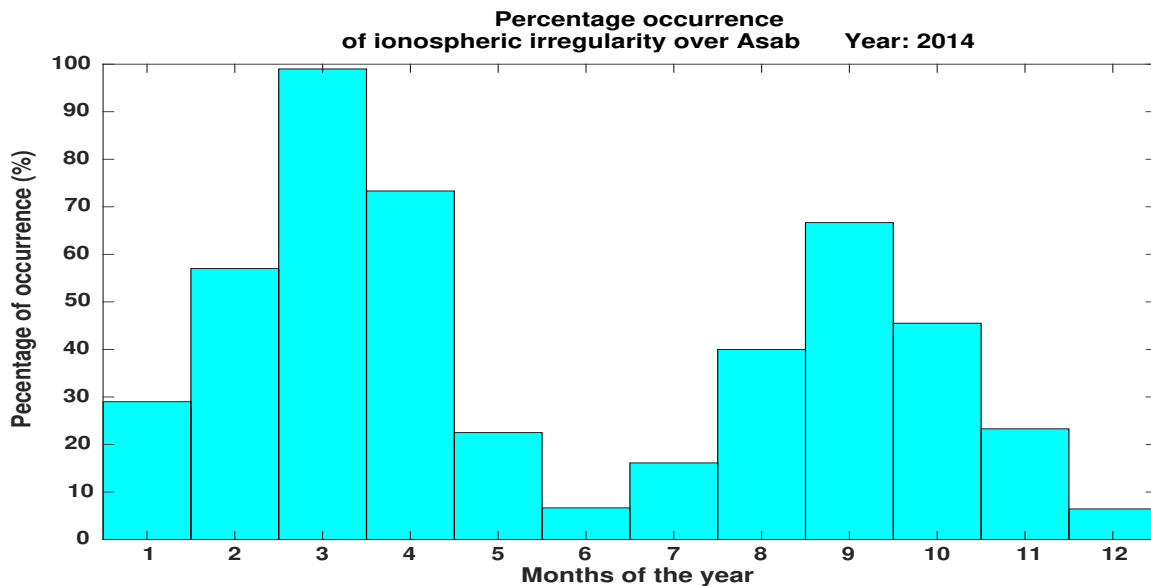
Figure 5. Percentage of occurrence of ionospheric irregularities over ASAB station during the year 2014 based on $ROTI_{ave}$ index.

1 In terms of local time, monthly, and seasonal behavior the enhancement in the spatial gradient of TEC and occurrence

2 of ionospheric irregularities show similar trends. And, it is evident from the above result that the spatial gradient of TEC

3 between two nearby stations where the two receivers lie nearly along the same latitudes could be used as an indicator

4 of the occurrence of large-scale ionospheric irregularities. In the current study, the minimum distance between the two

5 stations and the threshold value of the gradient of TEC that could indicate the probability of occurrence of ionospheric

6 irregularities has not been seen and needs further investigation.

7 **4 Conclusions**

8 In this study, we present the possibility that the spatial gradient of TEC between two nearby stations (ASAB and DEBK)

9 over East African sector could be used as indicator of the occurrence of large-scale ionospheric irregularities. The following

10 features were observed from the study. Most of the daily maximum positive/negative value of the spatial gradient of TEC

11 was observed in the pre-midnight and post-midnight period. In terms of seasons, months and local times, the maximum

12 positive of the spatial gradient of TEC and $ROTI_{ave}$ show similar tends. Both of them show enhancement during the

13 months of March and September equinoxes. Seasonal asymmetry was also observed in both parameters, where March

14 equinox was greater than September equinox. Peak values in the spatial gradient of TEC and $ROTI_{ave}$ was observed

15 about 1-2 hrs later from post-sunset enhancement of equatorial electric field (EEF). There is also a case where the

16 depletions of the gradient of TEC shows similar trends as the positive maximum value of the TEC gradient. Based on

17 the above results, the spatial gradient of TEC between the two nearby stations which lies along the same geographic and

1 geomagnetic latitudes could be used as an indicator of the occurrence of large-scale ionospheric irregularities. In this study,

2 we have also used the equatorial electric field model to relate the spatial gradient of TEC with the phase fluctuation index

3 ($ROTI_{ave}$). The threshold value of the gradient of TEC and the minimum separation distance between stations were not

4 presented in the current study and this will be considered in the future investigation.

Acknowledgments

6 The Authors would like to express their gratitude to the International GNSS Service (IGS) for providing the GPS data

7 and downloaded from the website: ftp://cddis.gsfc.nasa.gov. We acknowledge http://www.geomag.org/models/PPEFM/

8 RealtimeEF.html for providing the data the Prompt penetration equatorial electric field model. We also thank the AMBER

9 and INTERMAGNET magnetometer data centers for providing magnetometer data.

1 References

2 Aarons, J.: Construction of a model of equatorial scintillation intensity., Radio Sci., 20(3), 397-402,
3 https://doi.org/http://dx.doi.org/10.5194/angeo-32-7-2014, 1985.

4 Aarons, J.: The longitudinal morphology of equatorial F layer irregularities relevant to their occurrence., Space Sci. Rev., 63, 209.,
5 1993.

6 Aarons, J., Mendillo, M., and Yantosca, R. G.: GPS phase fluctuations in the equatorial region during sunspot minimum., Radio
7 Sci.., 32, 1535-1550., 1997.

8 Abadi, P., Otsuka, Y., and Tsugawa, T.: Effects of pre-reversal enhancement of E× B drift on the latitudinal extension of plasma
9 bubble in Southeast Asia, Earth, Planets and Space, 67, 74, 2015.

10 Abdu, M.: Outstanding problems in the equatorial ionosphere-thermosphere electrodynamics relevant to spread F., J. Atmos. Solar-
11 Terr. Phys., 63, 869-884, 2001.

12 Abdu, M. A., Bittencourt, J. A., and Batista, I. S.: Magnetic declination control of the equatorial F region dynamo field development
13 and spread F., J. Geophys Res. (USA), 86, 11443, 1981.

14 Abdu, M. A., Batista, I. S., Rios, V. H., and Medina, C.: Equatorial spread F occurrence statistics in the American longitudes:
15 Diurnal, seasonal and solar cycle variations., Adv. Space Res., 22(6), 851-854, 1998.

16 Abdu, M. A., Batista, I. S., Takahashi, H., MacDougall, J., Sobral, J. H., Medeiros, A. F., and Trivedi, N. B.: Magnetospheric
17 disturbance induced equatorial plasma bubble development and dynamics: A case study in Brazilian sector., J. Atmos. Solar-Terr.
18 Phys., 108(A12), 1449, https://doi.org/10.1029/2002JA009721, 2003.

19 Abdu, M. A., . Batista, I. S., Reinisch, B. W., de Souza, J. R., Sobral, J. H. A., Pedersen, T. R., Medeiros, A. F., Schuch, N. J., and
20 de Paula, E. R., a. G. K. M.: Conjugate Point Equatorial Experiment (COPEX) campaign in Brazil: Electrodynamics highlights on
21 spread development conditions and day to day variablity, J. Geophys. Res., 114, A04308, https://doi.org/10.1029/2008JA013749,
22 2009.

23 Amabayo, E., Jurua, E., Cilliers, P., and Habarulema, J.: Climatology of ionospheric scintillations and TEC trend over the Ugandan
24 region. , Adv. Space Res., 53,734-743., 2014.

25 Anderson, D., Anghel, A., Yumoto, K., Ishitsuka, M., and Kudeki, E.: Estimating daytime vertical $E \times B$ drift ve-
26 locities in the equatorial F-region using ground-based magnetometer observations, Geophys. Res. Lett., 29(12), 1596,
27 https://doi.org/10.1029/2001GL014562, 2002.

28 Anderson, D., Anghel, A., Chau, J., and Veliz, O.: Daytime vertical E× B drift velocities inferred from ground-based magnetometer
29 observations at low latitudes, Space Weather, 2, 2004.

30 Basu, S. and Basu, S.: Equatorial scintillations-A review, Journal of Atmospheric and Terrestrial Physics, 43, 473–489, 1981.

31 Basu, S., MacKenzie, E., and Basu, S.: Ionospheric constraints on VHF/UHF communications links during solar maximum and
32 minimum periods.

33 Basu, S., Kudeki, E., Basu, S., Valladares, C., Weber, E., Zengingonul, H., Bhattacharyya, S., Sheehan, R., Meriwether, J., Biondi,
34 M., Kuenzler, H., and Espinoza, J.: Scintillations, plasma drifts, and neutral winds in the equatorial ionosphere after sunset, J.
35 Geophys Res, 101, 26795-26809, 1996.

36 Batista, I., Abdu, M., and Bittencourt, J.: Equatorial F region vertical plasma drifts: Seasonal and longitudinal asymmetries in the
37 American sector, Journal of Geophysical Research: Space Physics, 91, 12 055–12 064, 1986.

1 Burke, W. J., Gentile, L. C., Huang, C. Y., Valladares, C. E., and Su, S. Y.: Longitudinal variability of equatorial plasma bubbles
2   observed by DMSP and ROCSAT-1, J. Geophys. Res., 19, https://doi.org/10.1029/2004JA010583, 2004.

3 Chu, F., Liu, J.Y., a. T. H., Sobral, J., Taylor, M., and Medeiros, A. F.: The climatology of ionospheric plasma bubbles and
4   irregularities over Brazil, Annales Geophysical, 23: 379-384, 2005.

5 Crain, D., Heelis, R., and Bailey, G.: Effects of electrical coupling on equatorial ionospheric plasma motions: When is the F region
6   a dominant driver in the low-latitude dynamo?, Journal of Geophysical Research: Space Physics, 98, 6033–6037, 1993.

7 Dabas, R. S., Singh, L., Lakshmi, D. R., Subramanyam, P., Chopra, P., and Garg, S. C.: Evolution and dynamics of equatorial
8   plasma bubbles: Relationships to ExB drift, postsunset total electron content enhancements, and equatorial electrojet strength.,
9   Radio Sci., 38(4), 1075, https://doi.org/10.1029/2001RS002586., 2003.

10 Dasgupta, A., Anderson, D., and Klobuchar, J.: Equatorial F-region ionization differences between March and September, Adv.
11   Space Res., 10, 199-202, 1983.

12 Farley, D., Balsey, B., Woodman, R., and McClure, J.: Equatorial spread F: Implications of VHF radar observations, Journal of
13   Geophysical Research, 75, 7199–7216, 1970.

14 Farley, D. T., Bonelli, E., Fejer, B. G., and Larsen, M. F.: The prereversal enhancement of the zonal electric field in the equatorial
15   ionosphere., J. Geophys. Res., 113,A05304., 2008.

16 Fejer, B.: Low latitude electrodynamics plasma drifts: a review., J. Atmos. Terr. Phys., 53, 677-693, 1991.

17 Fejer, B., Jensen, J., and Su, S.: Quiet time equatorial F region vertical plasma drift model derived from ROCSAT-1 observations.,
18   J. Geophys. Res., https://doi.org/http://dx.doi.org/10.1029/2007JA012801., 2008.

19 Fejer, B. G.: Low latitude ionospheric electrodynamics, Space Science Reviews, 158, 145–166, 2011.

20 Fejer, B. G., Scherliess, L., and de Paula, E. R.: Effects of the vertical plasma drift velocity on the generation and evolution of
21   equatorial spread F, J. Geophys. Res., 104, 19,859-19,869, https://doi.org/10.1029/1999JA900271, 1999.

22 Haerendel, G. and Eccles, J.: The role of the equatorial electrojet in the evening ionosphere, Journal of Geophysical Research: Space
23   Physics, 97, 1181–1192, 1992.

24 Hajra, R., Chakraborty, S., Mazumdar, S., and Alex, S.: Evolution of equatorial irregularities under varying electrodynamical condi-
25   tions: a multitechnique case study from Indian longitude zone, Journal of Geophysical Research: Space Physics, 117, 2012.

26 Horvath, I. and Essex, E.: Vertical E× B drift velocity variations and associated low-latitude ionospheric irregularities investigated
27   with the TOPEX and GPS satellite data, in: Annales Geophysicae, vol. 21, pp. 1017–1030, 2003.

28 Iyer, K., Souza, J., Pathan, B., Abdu, M., Jivani, M., and Joshi, H.: A model of equatorial and low latitude VHF scintillation in
29   India, Indian J. Radio Space Phys., 35, 98-104., 2006.

30 Kelley, M.: The Earth's Ionosphere: Plasma Physics and Electrodynamics, London, 1989.

31 Kelley, M. C.: The Earth's ionosphere: plasma physics and electrodynamics, vol. 96, Academic press, 2009.

32 Kintner, P., Ledvina, B., and Paula, E.: GPS and ionospheric scintillations, Space Weather, 5, S09003,
33   https://doi.org/http://dx.doi.org/10.1029/2006SW000260, 2007.

34 Ma, G. and Maruyama, T.: A super bubble detected by dense GPS network at East Asian longitudes., Geophys. Res. Lett., 133,
35   L21103, 2006.

36 Manju, G ., e. a.: Equinoctial asymmetry in the occurrence of equatorial spread-F over Indian longitudes during moderate to low
37   solar activity period., Indian J. Radio Space Phys, 41, 240-246, 2013.

1 Manju, G. and Haridas, M. M.: On the equinoctial asymmetry in the threshold height for the occurrence of equatorial spread F., J.
2   Atmos. Sol.Terr. Phys., 124, 59-62, 2015.

3 Manju, G., Devasia, C., and Ravindran, S.: The seasonal and solar cycle variations of electron density gradient scale length, vertical
4   drift and layer height during magnetically quiet days: Implications for Spread F over Trivandrum, India, Earth, planets and space,
5   61, 1339–1343, 2009.

6 Manoj, C. and Maus, S.: A real-time forecast service for the ionospheric equatorial zonal electric field., Space Weather, 10,
7   https://doi.org/http://dx.doi.org/10.1029/2012SW00082, 2012.

8 Martinis, C. R., Mendillo, M. J., and Aarons, J.: Toward a synthesis of equatorial spread F onset and suppression during geomagnetic
9   storms, J. Geophys. Res., 110, A07306, https://doi.org/10.1029/2003JA010362, 2005.

10 Maruyama, T., Saito, S., Kawamura, M., Nozaki, K., Krall, J., and D.Huba, J.: Equinoctial asymmetry of a low-latitude
11   ionosphere-thermosphere system and equatorial irregularities: Evidence for meridional wind control., Ann. Geophys., 27, 2027-
12   2034, https://doi.org/10.5194/angeo-27-2027-2009, 2006.

13 Mendillo, M., Lin, B., and Aarons, J.: The application of GPS observations to equatorial aeronomy., Radio Sci., 35, 885-904., 2000.

14 Mendillo, M., Meriwether, J., and Biondi, M.: Testing the thermospheric neutral wind suppression mechanism for day-to-day
15   variability of equatorial spread F., J. Geophys. Res., 106, 3655., 2001.

16 Mungufeni, P., Jurua, E., Habarulema, J., and Anguma, S.: Modelling the probability of ionospheric irregularity occurrence over
17   African low latitude region., J. Atmos. Solar Terr. Phys., 128, 46-57, 2015.

18 Mungufeni, P., Jurua, E., and Habarulema, J.: Trends of ionospheric irregularities over African low lat-
19   itude region during quiet geomagnetic conditions., J. Atmos. Solar Terr. Phys., 138-139, 261-267,
20   https://doi.org/http://dx.doi.org/10.1016/j.jastp.2016.01.015, 2016.

21 Mushini, S. C., P. T. J. R. B. L. J. W. M. and Pokhotelov, D.: Improved amplitude and phase scintillation indices derived from
22   wavelet detrended high latitude GPS data, PS Solut., https://doi.org/10.1007/s10291-011-0238-4, 2011.

23 Nayak, C., Tsai, L.-C., Su, S.-Y., Galkin, I., Caton, R., and Groves, K.: Suppression of ionospheric scintillation during St. Patrick's
24   Day geomagnetic super storm as observed over the anomaly crest region station Pingtung, Taiwan: A case study, Advances in
25   Space Research, 60, 396-405, https://doi.org/http://dx.doi.org/10.1016/j.asr.2016.11.036, 2017.

26 Ngwira, C. M., Klenzing, J., Olwendo, J., D'ujanga, F. M., Stoneback, R., and Baki, P.: A study of intense ionospheric scintillation
27   observed during a quiet day in the East African low-latitude region, Radio Sci., 48, 396-405,, https://doi.org/10.1002/rds.20045,
28   2013.

29 Nishioka, M., Saito, A., and Tsugawa, T.: Occurrence characteristics of plasma bubble derived from global ground-based GPS
30   receiver networks, J. Geophys. Res., 113, A05301, https://doi.org/10.1029/2007JA012605, 2008.

31 Oladipo, O. A. and Schuler, T.: Magnetic storm effect on the occurrence of ionospheric irregularities at an equatorial station in the
32   African sector, Ann.Geophys., 56, 5, A0565, https://doi.org/10.4401/ag-6247, 2013a.

33 Oladipo, O. A. and Schuler, T.: Equatorial ionospheric irregularities using GPS TEC derived index., Atmos. Sol. Terr. Phys., 92,
34   78-82., 2013b.

35 Oladipo, O. A., Adeniyi, J. O., Olawepo, A. O., and Doherty, P. H.: Large-scale ionospheric irregularities occurrence at Ilorin,
36   Nigeria, Space Weather., 12, 300-305., https://doi.org/10.1002/2013SW000991, 2014.

1 Olwendo, O., Baluku, T., Baki, P., Cilliers, P., Mito, C., and Doherty, P.: Low latitude ionospheric scintillation and zonal irregularity
2   drifts observed with GPS-SCINDA system and closely spaced VHF receivers in Kenya, Adv. in Space Res., 51, 1715-1726.,
3   https://doi.org/http://dx.doi.org/10.1016/j.asr.2012.12.017, 2013.

4 Olwendo, O., Baki, P., Cilliers, P., Doherty, P., and Radicella, S.: Low latitude ionospheric scintillation and zonal plasma irregularity
5   drifts climatology around the equatorial anomaly crest over Kenya, J. Atmo. Solar-Terr. Phys., 138-139, 9-22., 2016.

6 Otsuka, Y., Shiokawa, K., and Ogawa, T.: Equatorial ionospheric scintillations and zonal irregularity drifts observed with closely
7   spaced GPS receivers in Indonesia., J. Meteorol. Soc. Jpn., 84A, 343-351, 2006.

8 Paznukhov, V., Carrano, C., Doherty, P., Groves, K., Caton, R.G., a. V. C., Seemala, G., Bridgwood, C., Adeniyi, J., Amaeshi,
9   L., Damtie, B., a. D. M. F., Ndeda, J., Baki, P., Obrou, O., Okere, B., and Tsidu, G.: Equatorial plasma bubbles and L-band
10   scintillations in Africa during solar minimum., Ann. Geophys., 30, 675-682, 2012.

11 Pi, X., Mannucci, A. J., Lindqdwister, U. J., and Ho, C.: Monitoring of Global Ionospheric Irregularities using the worldwide GPS,
12   Geophys. Res. Lett., 24, 2283-2286, https://doi.org/10.1029/97GL02273, 1997.

13 Rao, P. R., Krishna, S. G., Niranjan, K., and Prasad, D.: Study of spatial and temporal characteristics of L-band scintillations over
14   the Indian low-latitude region and their possible effects on GPS navigation, in: Annales Geophysicae, vol. 24, pp. 1567–1580,
15   2006.

16 Rastogi, R. G. and Klobuchar, J. A.: Ionospheric electron content within the equatorial F2 layer anomaly belt., J. Geophys. Res,
17   95(A11),19,045-19,052, 1990.

18 Rishbeth, H.: Polarization fields produced by winds in the equatorial F-region, Planetary and Space Science, 19, 357–369, 1971.

19 Rungraengwajiake, S., Supnithi, P., Saito, S., Siansawasdi, N., and Saekow, A.: Ionospheric delay gradientmonitoring for GBAS by
20   GPS stations near Suvarnabhumi airport, Thailand., Radio Sci., 50, 1076-1085, https://doi.org/10.1002/2015RS005738, 2015.

21 Saito, S. and Yoshihara, T.: Evaluation of extreme ionospheric total electron content gradient associated with plasma bubbles for
22   GNSS Ground-Based Augmentation System, Radio Science, 52, 951-962, 2017.

23 Scherliess, L. and Fejer, B.: Radar and satellite global equatorial F region vertical drift model, J. Geophys. Res., 104 (4A), 6829-6842,
24   1999.

25 Seba, E. and Tsegaye, K. G.: Characterization of ionospheric scintillation at a geomagnetic equatorial region station., Adv. Space
26   Res., 56, 2057-2063, 2015.

27 Seemala, G. and Valladares, C.: Statistics of total electron content depletions observed over the South American continent for the
28   year 2008, Radio Science, 46, RS5019, 2011.

29 Sreeja, V., Devasia, C., Ravindran, S., and Pant, T. K.: Observational evidence for the plausible linkage of Equatorial Electrojet
30   (EEJ) electric field variations with the post sunset F-region electrodynamics, in: Annales geophysicae: atmospheres, hydrospheres
31   and space sciences, vol. 27, p. 4229, 2009.

32 Sripathi, S., Kakad, B., and Bhattacharyya, A.: Study of equinoctial asymmetry in the Equatorial Spread F (ESF) irregularities
33   over Indian region using multi-instrument observations in the descending phase of solar cycle 23, J. Geophys. Res., 116, A11302,
34   https://doi.org/10.1029/2011JA016625., 2011.

35 Susnik, A. and Forte, B.: Ionospheric scitillation activity measured in the African sector, paper presented at General Assembly and
36   Scientific Symposium, XXXth URSI, Istanbul, Turkey., 2011.

37 Taabu, S., D'ujanga, F., and Ssenyonga, T.: Prediction of ionospheric scintillation using neural network over East African region
38   during ascending phase of sunspot cycle 24, Adv. Space Res., https://doi.org/http://dx.doi.org/10.1016/j.asr.2016.01.014, 2016.

1 Tsunoda, R.: Control of the seasonal and longitudinal occurrence of equatorial scintillations by the longitudinal gradient in integrated
2   E region Pederson conductivity., J. Geophys. Res., 90, 447., 1985.
3 Tsunoda, R. T.: On the enigma of day-to-day variability in Wave structure in equatorial Spread F, Geophys. Res. Lett., 32, 2005.
4 Tsunoda, R. T.: On seeding equatorial spread F during solstices, Geophys. Res. Lett., 37, L05102.,
5   https://doi.org/http://dx.doi.org/10.1029/2010GL042576., 2010.
6 Tulasi Ram, S., Rao, P. V. S. R., Niranjan, K., Prasad, D. S. V. V. D., Sridharan, R., Devasia, C. V., and Ravindran, S.: The role
7   of post-sunset vertical drifts at the equator in predicting the onset of VHF scintillations during high and low sunspot activity
8   years., Ann. Geophys., 24, 1609-1616, 2006.
9 Valladares, C., Basu, S., Groves, K., Hagan, M., Hysell, D., Mazzella Jr., A., and Sheehan, R.: Measurement of the latitudinal
10   distribution of total electron content during equatorial spread-F events, J. Geophys. Res., 106, 29133-29152, 2001.
11 Valladares, C., Villalobos, J., Sheehan, R., and Hagan, M.: Latitudinal extension of low-latitude scintillations measured with a
12   network of GPS receivers, Ann. Geophys., 22, 3155-3175, 2004.
13 Whalen, J. A.: The equatorial anomaly: Its quantitative relation to equatorial bubbles, bottomside spread F, and $E \times B$ drift velocity
14   during a month at solar maximum, Journal of Geophysical Research: Space Physics, 106, 29 125–29 132, 2001.
15 Woodman, R.: Vertical drift velocities and East-West electric fields at the magnetic equator., J. Geophys. Res., 75(31), 6249-6259,
16   https://doi.org/10.1029/JA075i031p06249, 1970.
17 Yizengaw, E. and Moldwin, M. B.: African Meridian B-field Education and Research (AMBER) array., Earth Moon Planet, 104,
18   237-246, https://doi.org/10.1007/s11038-008-9287-2, 2009.
19 Yizengaw, E., Moldwin, M. B., Zesta, E.and Biouele, C. M., Damtie, B., Mebrahtu, A., Rabiu, B., Valladares, C. F., and Stoneback,
20   R.: The longitudinal variability of equatorial electrojet and vertical drift velocity in the African and American sectors., Ann.
21   Geophys., 32, 231-238, 2014.